2022 IEEE 5th International Conference on Soft Robotics (RoboSoft)
April 4-8, 2022, Edinburgh, UK

Development and Characterization of a Soft Valve for Automatic Fault Isolation in Inflatable Soft Robots

Marco Pontin[1], Shuhei Miyashita[1] and Dana D. Damian[1]

Abstract— **Common causes of failure of inflatable soft robots are bursts due to wear, overpressurization or interactions with their surroundings. Resilience, the ability to survive such faults, is key for autonomous robotic systems, especially when human intervention is impossible or risky (e.g. robotic implants or space exploration). Although self-healing has been investigated as a possible solution, the approaches presented to date still have critical limitations. In this paper, we present a novel resilience mechanism based on soft valves. When used with soft actuators consisting of multiple inflatable segments connected in parallel, these are designed to readily isolate a burst section before the fault can propagate to the rest of the system. No additional sensing is required. The shut-off action of the valve is triggered by the pressure difference caused by the fault itself, as proved in the final application. The valve takes less than 30 ms to switch and can operate at various pressure levels: supply pressures up to 15 kPa were tested. This fault-isolating soft valve represents a new step towards soft robotic resilience, addressing soft robots vulnerabilities in difficult-to-access sites or in settings of high-risk for the system or its surroundings.**

I. INTRODUCTION

In the last decade, soft robotics has become an important and popular area of research. Soft robots have demonstrated interesting and unique capabilities: growing bodies, better ability in coping with unstructured environments, ability to survive large deformations [1], [2], [3]. Using soft materials, researchers have been able to develop actuators [4], [5], [6], sensors [4], [7], [8], and controllers [9], [10]. Their softness, though, makes them prone to failure when interacting with the surroundings or to burst if overpressurized. Repeated inflation and wear due to contact can also lead to the same result. These are all common failure modes of fluidic soft actuators and, as such, they represent a critical shortcoming for their application in robotic systems, especially in cases where autonomy and ability to overcome faults are paramount, such as robots for search and rescue, space exploration or medical robotic implants. In all of these cases, there is the necessity for the systems to autonomously detect, isolate and eventually solve potential faults, as human intervention is either impossible or very risky. Key work to overcome this problem has been carried out in the field of self-healing materials. Researchers have realized composite materials, capable of sensing and actuation, that show functional self-healing capabilities [11], [12], [13]. Focusing on inflatable soft-robots, Terryn et al. demonstrated the use of self-healing polymer-sheets to build actuators that can recover macroscopic damage [14]. A similar result was achieved by Shepard et al. using an Ecoflex™-Kevlar composite [15] and by Wallin et al. [16] through a thiol–ene click chemistry. These approaches, although promising, still show limitations. In the majority of the cases, the focus is on the chemical process itself and not on how this affects the performance of the system while healing or on the fault detection aspect. Specific materials need to be used to exploit self-healing and the self-healing process itself can require from tens of seconds to several hours to complete. Meanwhile, the actuators need to be deflated or leakage of actuation fluid occurs. Sometimes, particular environmental conditions are needed for the process to occur, such as the presence of a UV source or an increase in ambient temperature. Most importantly though, these techniques can only recover relatively small damages, such as punctures and neat cuts, where no original material is removed. This leaves the necessity of finding ways to isolate the faulty section of the robot, either temporarily, while the fault is healing, or permanently, if the damage is unrecoverable, as not doing so could cause loss of functionality for prolonged or indefinite periods of time. Also, when multiple segments of the actuator are connected to the same supply line, one burst could lead the entire soft robot to fail. Even when a powerful supply line is present, that can cope with the outflow of actuation fluid, this translates in an overall bulkier system and in a waste of critical resources in untethered applications.

In this article, we present a novel automatic fault detection and isolation technique for inflatable soft robots, based on pressure-difference triggered soft valves. The integration of soft valves has recently been used for control purposes to create fully soft robots [10], [17], [18]. Still, little work has been devoted to fault detection and isolation. The goal of this work is to develop and characterize a pneumatic soft valve that enables sensing and isolation of bursts, with no controller intervention. The envisaged application is to create a distributed fault isolation network for inflatable soft actuators with multiple chambers connected together (Section IV). The result is a potential reduction in pneumatic supply lines as well as external sensing elements and valves to achieve similar functionality.

II. DESIGN AND FABRICATION

The soft valve consists of three main parts: the flow layer, containing the main flow channel that connects the supply line with the soft actuator, the control layer, where

*This work was supported by the EPSRC under Grant EP/S021035/1, and EPSRC ERC DTP Scholarship. Data available on the ORDA doi 10.15131/shef.data.19419602.

[1]M. Pontin, S. Miyashita and D. D. Damian are with the Automatic Control and Systems Engineering Department, University of Sheffield, Sheffield, UK (e-mail: mpontin1@sheffield.ac.uk, d.damian@sheffield.ac.uk).

2022 IEEE 5th International Conference on Soft Robotics (RoboSoft) | 978-1-6654-0828-8/22/$31.00 ©2022 IEEE | DOI: 10.1109/ROBOSOFT54090.2022.9762134

the control chamber is located, and the membrane, which separates the two (Fig.1(a)). Although the design of the valve originates from Quake-style valves [19], [20], the proposed valve's novelty stems from the distinct structural materials and working principle. Ecoflex™ 00-50 is used in the final application, leading to a much softer valve compared to traditional PDMS Quake valves. In addition, while Quake valves rely on a static uniform pressure difference to operate, our design exploits the dynamic creation of a pressure gradient in the flow channel caused by the burst. Key for this behaviour is the restriction in the flow layer, underneath the control chamber. The geometry produces two effects: it creates a disconnect between the inlet and the outlet, acting as a concentrated pneumatic resistance, and it reduces the distance the membrane needs to deform to shut off the flow, meaning a lower pressure difference Δp is required for the valve to switch, therefore reducing the response time of the component. The channels have square section of height H, that reduces down to a minimum height h where the raised section of the flow channel is. The control chamber, and the membrane as a result, is circular with diameter D. Finally, the membrane is characterized by its thickness t (Fig.1(b)).

Two prototypes of the valve were manufactured, one made out of PDMS silicone (Sylgard™ 182) and the second using Ecoflex™ 00-50. Molds for all the parts were fabricated using a Formlabs Form 2 SLA printer with the layer height set to 25 μm. Fig.1(a) summarizes the steps of the manufacturing process. After molding and degassing, the Ecoflex™ components were cured in an oven (SciQuip 80-HT) at 75 °C for 25 minutes, demolded and then irreversibly bonded using Sil-poxy™ glue. The PDMS parts were cured at 125 °C for 30 minutes and bonded in pairs using oxygen plasma coating (Henikker Plasma HPT-200): air was used as process gas, the flow in the chamber was set to 20 sccm, the power to 100% and the samples were exposed for 55 s. Immediately after exposure to plasma, the parts were firmly pressed together for 60 s and then placed for 10 minutes on a hotplate set to 90 °C. This study will mostly focus on the Ecoflex™ 00-50 version of the valves as the material properties better reflect those typically seen in inflatable soft robots. PDMS samples are used during the experimental characterization phase as a reference: the manufacturing technique together with the higher stiffness of the material lead to more precise samples with little to no internal deformation upon pressurization.

III. FINITE ELEMENT ANALYSIS

Finite element analysis (FEA) was used to select an appropriate thickness t for the membrane. Before performing the analysis in Abaqus, uniaxial tensile tests were conducted for material characterization. Ecoflex™ 00-50 dog bone samples were molded according to the manufacturing process just presented and an Ogden model with $N = 1$ (1) was chosen to fit the model parameters to the experimental data (Fig.2(a)). Three out of ten tensile tests were used for the estimation of the material properties.

$$\sigma_{uniax} = \frac{2\mu}{\alpha}\left(\lambda^{\alpha} - \lambda^{-\frac{1}{2}\alpha}\right) \qquad (1)$$

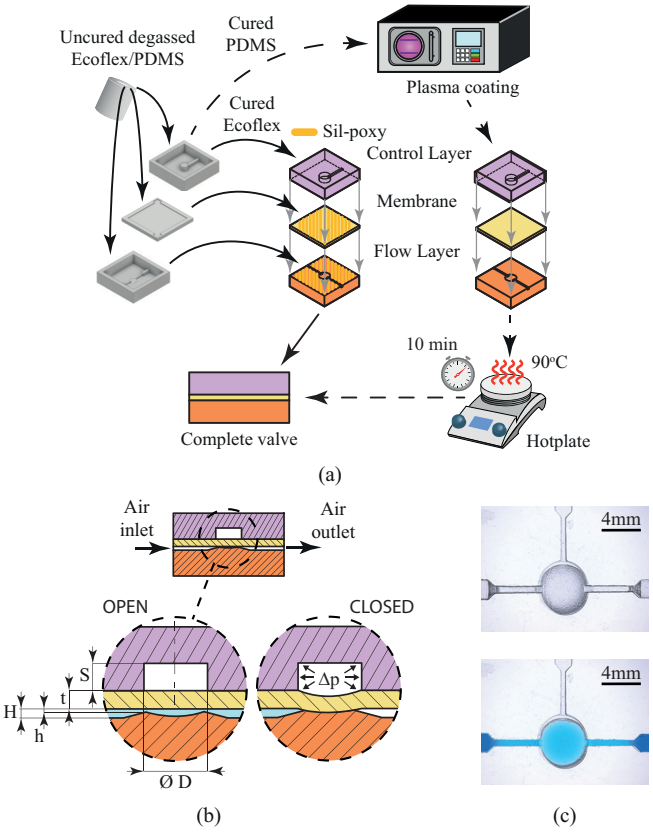

Fig. 1. Manufacturing process of the soft valve. (a) Two versions are realized using Ecoflex™ 00-50 and Sylgard™ 182. Ecoflex parts are irreversibly bonded using Sil-poxy™ glue, while oxygen plasma is used for the Sylgard™ 182 ones. (b) Sections of the open and closed soft valve with relevant dimensions. (c) Top view of a PDMS valve. The flow channel is highlighted using colored liquid.

In the equation, σ_{uniax} represents the stress and λ the strain. Fitting in Abaqus resulted in $\mu = 0.0263$ and $\alpha = 3.093$. To validate the material model, samples were built, consisting only of the control layer and the membrane, and pressurized. The experimental results were then compared to the simulations at various levels of inflation. The maximum height of the deformed membrane was used as the metric for the comparison and two membrane thicknesses were considered: 500 μm and 1 mm. Fig.2(b) shows a summary of the comparison. For the experiments, three different samples were used per each thickness and the results were then averaged. The simulated displacement proved to be in line with the experimental one, with slightly bigger discrepancies for larger deformations. The maximum error was 0.34 mm for the 500 μm at 15 kPa of internal pressure.

To guide the sizing of the membrane thickness for the valve, in line with preliminary experimental data, the assumption was made that when a burst occurs, in the flow channel, underneath the membrane, the pressure is given by the mathematical average between supply and ambient pressure. The pressure difference that causes the membrane to bend down is therefore equal to $p_{supply}/2$. One simulation of the complete valve can be seen in Fig.2(c). The flow channel

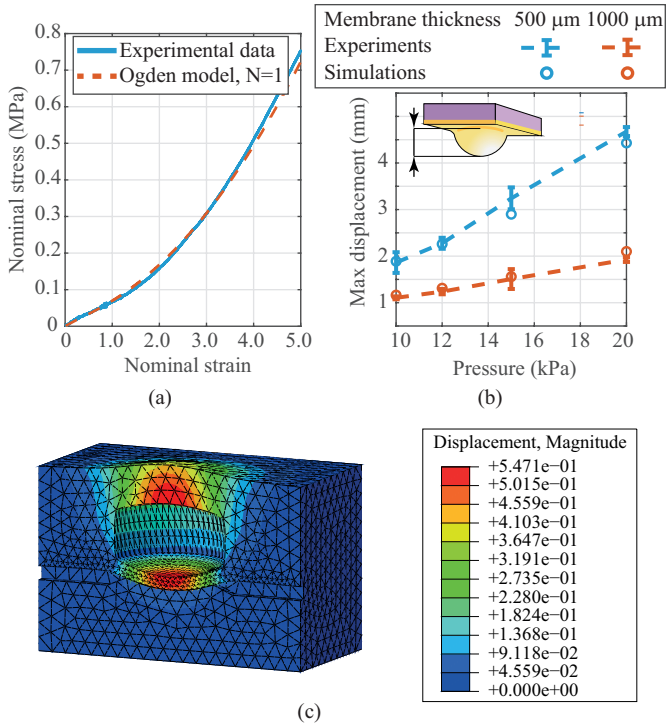

Fig. 2. FEA analysis of the valve. (a) Results of the tensile tests on Ecoflex™ 00-50 and fitting of the Ogden model. An Imada MX2 tensile testing machine was used at 50.0 mm/min. (b) Validation of Abaqus simulations using the height of the inflated membrane as metric. Two different membrane thicknesses were used and three samples per thickness were manufactured and tested at varying inflation levels. (c) Abaqus simulation of the complete Ecoflex™ 00-50 valve inflated at 7.5 kPa. Membrane thickness $t = 500\,\mu$m.

is at ambient pressure, while a uniform pressure of 7.5 kPa is present in the control chamber at the top, simulating a supply pressure $p_{supply} = 15$ kPa. The valve, with the 500 μm thick membrane, was modelled as monolithic for simplification and internal contacts were enabled in Abaqus to simulate the interaction between the membrane itself and the bottom of the flow channel. The complex interaction between the air flow in the flow layer and the membrane was neglected and will be analyzed in future studies. According to the simulations, a 500 μm thick membrane should be capable of deforming enough to fully obstruct the flow channel. This result was used as the baseline for the manufacturing of the soft valve.

IV. EXPERIMENTAL RESULTS

A. Characterization of the Flow Rate Through the Valves

To characterize the valves, flow rate tests were performed referring to ISO 6358. The experiments were conducted using the pneumatic circuit in Fig.3(a). The pressure inside the tank is kept constant using a PI controller, while the outflow is measured using an analogue air flow sensor. As visible in Fig.3(b) and (c), the tests are conducted on a version of the valve consisting of the flow channel and a solid top layer bearing miniature channels. These enable the insertion of syringe needles to measure the pressure right before (p_{in}) and after (p_{out}) the restriction in the flow channel. O-rings, embedded during the molding phase, provide sealing. Finally, a flow regulator is used to incrementally reduce p_{out}, from p_{supply} to ambient pressure. According to the ISO norm, the flow through a rigid valve can be expressed using (2).

$$\begin{cases} Q_N = C\sqrt{\frac{T_0}{T}}p_{in} & \text{if } \frac{p_{out}}{p_{in}} \leq b \\ Q_N = C\sqrt{\frac{T_0}{T}}p_{in}\sqrt{1-\left(\frac{\frac{p_{out}}{p_{in}}-b}{1-b}\right)^2} & \text{if } \frac{p_{out}}{p_{in}} > b \end{cases} \tag{2}$$

Pressures p are absolute and measured in bars, temperatures T are in K and Q_N, the flow rate, is expressed in Nls^{-1}. $T_0 = 293$ K is the reference temperature for normal conditions. The conductance C, measured in Nls^{-1}bar^{-1}, is directly proportional to the maximum flow rate through the valve at a given supply pressure p_{in}. Coefficient b represents the critical pressure ratio below which the flow reaches sonic speed and does not increase anymore when further decreasing the ratio p_{out}/p_{in}. It can be demonstrated that b has value 0.528 for an ideal nozzle in the absence of losses and is lower in real components, even reaching zero. In addition, in normal soft robotics applications the difference between absolute supply pressure and absolute ambient pressure is relatively small, leading to a ratio p_{out}/p_{in} close to 1. Because of these considerations, we assumed $b = 0$, leaving only the conductance to be experimentally determined.

Five different geometries of the flow channel were considered for both the Ecoflex™ and the PDMS versions of the valve: H varied in the range $[0.5, 1.0, 1.5]$ mm, while h was equal to 100 μm, 150 μm, and 200 μm for $H = 0.5$ mm and was 150 μm for $H = 1.0$ mm and $H = 1.5$ mm. All other dimensions of the flow channel were kept constant. Fig.3(d) and (e) show the results obtained with $H = 0.5$ mm and $h = 150\,\mu$m for the PDMS and Ecoflex™ versions respectively. As visible, the minimum value for the ratio p_{out}/p_{in} is 0.88 for $p_{in} = 15$ kPa, confirming our previous considerations on b. Also, contrary to the Ecoflex™ ones, flow curves for the PDMS valves overlap, reflecting what would be expected using fully rigid valves. This is also confirmed by the coefficient of variation σ/μ of the conductance C after fitting, whose average value is 0.08 for the PDMS samples and 0.30 for the Ecoflex™ ones. The difference in behavior of the valves can be ascribed to internal deformations of the softer Ecoflex™ samples when pressure is applied. These deformations lead to a wider flow channel with a resulting increase in the flow rate at any given ratio p_{out}/p_{in}. Fig.3(f) summarizes the results obtained with the various geometries: the conductance is expressed as a function of the minimum area of the flow layer. Ecoflex™ valves with an area greater than 0.1 mm^2 could not easily achieve p_{out} equal to ambient pressure due to their lower internal resistance. This made them unsuitable candidates for later sections of this study. Knowing the conductance makes it possible to select the appropriate geometry of the flow layer based on the application as well as being the first step towards a complete model of the valve. For the PDMS components, a second order polynomial provides a

good fitting of the experimental data points ($R^2 = 0.97$). The same cannot be done for the Ecoflex™ versions as the supply pressure level impacts the conductance. Modelling is made challenging by the non-linear behavior of the silicone material and the complex interaction between the evolving pressure gradient in the flow layer and the channel itself.

B. *Shut-off Operation*

When characterizing the shut-off capabilities of the valve, the pneumatic circuit of Fig.3(a) was altered as shown in Fig.4(a). A control line is now present, to switch the pressure in the control layer of the valve on and off. Also, the flow regulator is removed and an outlet valve is added downstream of the flow sensor used to measure the outflow.

Samples were created with $H = 0.5$ mm and $h = 150\,\mu$m, while the membrane thickness t was varied in the range $[100, 200, 300, 500]\,\mu$m. The supply pressure was increased in steps of 5 kPa from 5 kPa to 15 kPa and four samples were tested at each pressure level. Fig.4(b) displays the testing procedure in details and shows the results obtained with a $100\,\mu$m thick membrane. First, the desired supply pressure is stabilized inside the tank. Then, valve V1 is turned on, pressurizing the flow layer up to V2. This causes a small flow through the flow sensor, as visible in the bottom chart at the time $t = 1.00$ s. 150 ms later, V3 opens, pressurizing the control line. After 5 s, $V3$ is closed and V2 is opened, connecting the outlet of the soft valve to ambient pressure, thus simulating a sudden burst in a soft actuator ($t = 6.15$ s). The air trapped between the soft valve and V2 flows out, causing a peak in the flow meter reading. If the valve works correctly, no flow should be measured in the following 3 s (grayed out region in the bottom chart of Fig.4(b)). The duration of the second spike in the flow rate can be interpreted as an upper bound for the switching time of the valve and never exceeded 30 ms. At $t = 9.15$ s, V1 is closed and V4 is opened, depressurizing the control line and resetting the circuit to the initial state. Immediately after opening V3, the membrane goes back to its resting position and the air trapped between V1 and the soft valve discharges, causing the third peak in the flow meter readings.

Fig.4(c) presents the results, as an average of four trials, for the four membrane thicknesses and the three supply pressure levels. As visible, contrary to the FEA simulations, the $500\,\mu$m thick membrane could not seal the flow layer and air leakage occurred during the trials for all three supply pressure levels. This is likely caused by the interaction between the air flow and the membrane, as well as the internal deformations of the flow layer caused by the pressure. In addition, the outflow increased in absolute terms with the increasing inlet pressure. The same happened for the $300\,\mu$m membrane, but this time the measured flow was lower, implying that the membrane was obstructing a larger percentage of the cross section of the flow channel. Samples with $200\,\mu$m thick membranes were capable of blocking the outflow for a supply pressure of 5 kPa, but then failed to do so for higher pressure values. The valves with $100\,\mu$m thick membranes were the only ones that could completely and reliably seal the flow

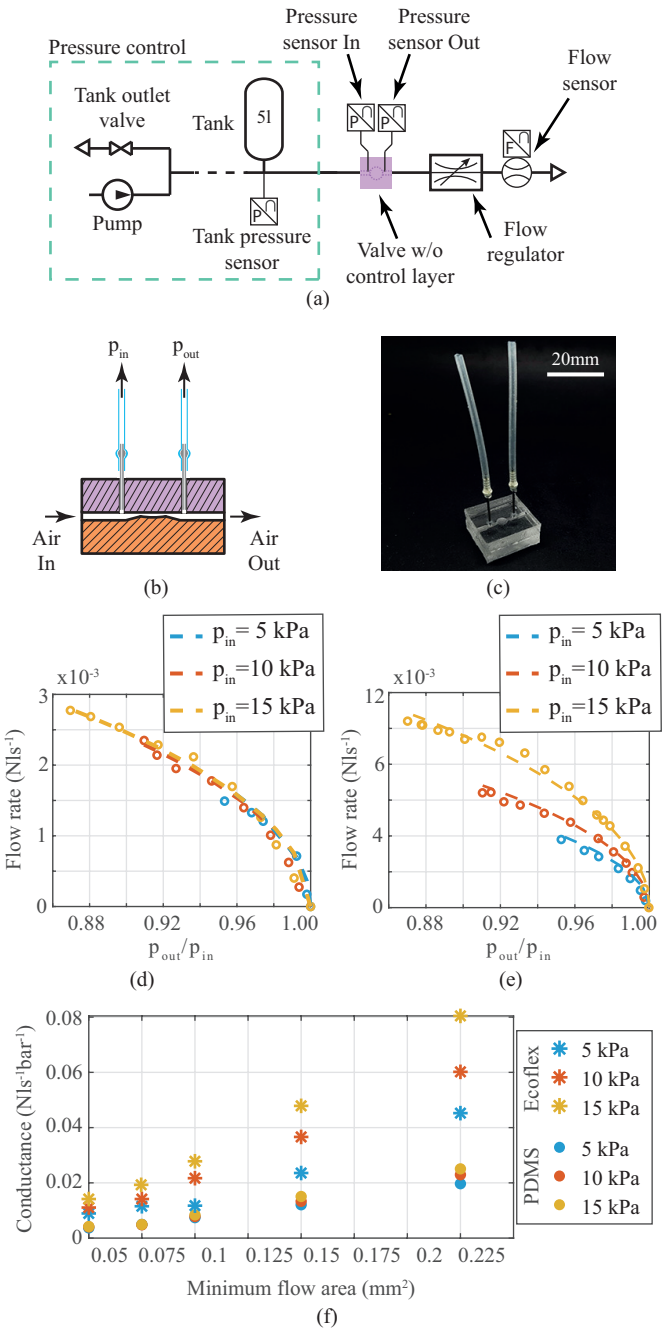

Fig. 3. Characterization of the flow rate through the soft valves. (a) Diagram of the pneumatic circuit used for the tests. (b) Section view of the component being tested. (c) Photograph of a PDMS sample: syringe needles are inserted for measuring the pressure inside the flow layer. (d) Characterization of a PDMS valve having $H = 0.5$ mm and $h = 150\,\mu$m. Three different supply levels were used in the range of typical soft robotics applications. Experimental data points are shown as circles, while dashed lines represent the fitting according to (2). (e) Characterization of an Ecoflex™ 00-50 valve having $H = 0.5$ mm and $h = 150\,\mu$m. The curves diverge due to internal deformations generated when the flow layer is pressurized. (f) Conductance of the valves as a function of the minimum area of the flow layer. Five different geometries were considered, varying both the width H and the height h of the channel. For any given geometry, the PDMS data points are closer together than the Ecoflex™ ones, highlighting the effect that the supply pressure level has on the softer material.

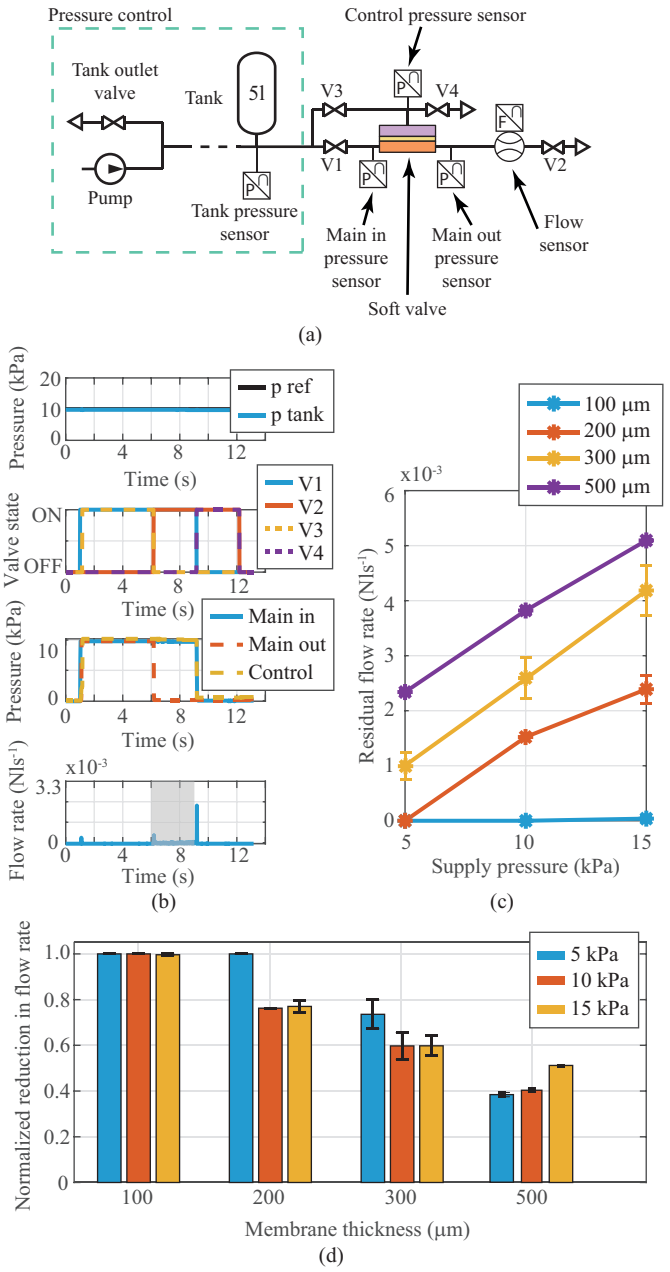

Fig. 4. Characterization of the shut-off capabilities of the soft valve. (a) Schematic of the pneumatic circuit used for the tests. (b) Experimental results obtained using a sample with $H = 0.5\,\text{mm}$, $h = 150\,\mu\text{m}$ and $t = 100\,\mu\text{m}$. The control layer is pressurized using an external valve (V3) 150 ms after the flow layer and is then isolated. The main outlet valve (V2) is later opened at $t = 6.15\,\text{s}$ to simulate a burst, but no outflow is observed (grayed out region in the bottom chart). Finally, the system is reset for the next test. The peaks in the flow rate correspond to the initial pressurization of the flow layer, to the discharge of the tubing between the soft valve and the outlet valve and to the discharge of the system during the reset phase. (c) Comparison of valves with same internal geometry and varying membrane thickness. The outflow was measured for varying levels of the supply pressure. Samples with $t = 100\,\mu\text{m}$ reliably succeeded in shutting off the flow completely, while ones with thicker membranes only reduced it partially. (d) Shut-off effectiveness of the valves for varying membrane thicknesses. The normalization was done using the maximum flow rate observed for the given geometry and supply pressure level during experiments such as that in Fig.3(e). Even when not fully blocking the outflow, the valves with $200\,\mu\text{m}$, $300\,\mu\text{m}$ and $500\,\mu\text{m}$ thick membranes were able to reduce the outflow by 80%, 60% and 40% respectively, compared to the membrane being absent.

layer all throughout the supply pressure range. The thinner membrane was capable of deforming enough to compensate for the internal deformations of the flow layer for all supply pressure levels. Even when not completely stopping the flow, the valves were still able to reduce it by more than 40% in the case of the $500\,\mu\text{m}$ membrane and up to 80% with the $200\,\mu\text{m}$ one, as summarized in the bar chart of Fig.4(d). The normalized reduction in flow rate (NRF) was chosen as the metric to compare the effectiveness of the various samples. The normalization was done using the following formula.

$$NRF = \frac{Q_{max} - Q_{out}}{Q_{max}} \tag{3}$$

Q_{out} is the outflow measured during the test and Q_{max} is the maximum flow rate achieved for the specific supply pressure level and channel geometry during the characterization experiments of Fig.3(e), where the membrane was absent. Overall, the valves proved to be effective and future work will focus on optimizing the internal geometry.

C. Application Example

To prove the effectiveness of the proposed design in real world applications, the soft-rigid actuator presented in [21] was used. These actuators consist of ring-shaped stackable modules, each having three independently inflatable membranes. As shown in Fig.5 and in the supplementary video, one module and three valves (V1, V2 and V3) were utilized for the demo. Each valve is connected to the common supply line and V1 is also connected to the control line. Valves V2 and V3 are passive and are only used to get similar amounts of pneumatic resistance in all three lines to the inflatable membranes (M1, M2 and M3). The decision of having only one fully connected valve was done to better highlight the behavior and effect that the valve, V1 in this case, has on the system. All three valves have $H = 0.5\,\text{mm}$, $h = 150\,\mu\text{m}$ and a $100\,\mu\text{m}$ thick membrane inside.

The actuator in its deflated state is shown in Fig.5(a), with V1 switched off. The supply line is then pressurized and the actuator inflates (Fig.5(b)). In the experiment, a supply pressure of 10 kPa was used. Right after inflation, the control line of valve V1 is turned on, pressurizing the control layer and preparing the membrane to snap down in case of a fault in the inflatable membrane M1. The system is then completely isolated from the supply, by disconnecting the external rigid valves, so that the pump cannot provide any more air to the inflatable membranes. A precision knife is used to burst the actuator, but membranes M2 and M3 remain inflated (Fig.5(b) and (c)). One minute after the burst, the actuator was still inflated, with no visible change in inflation level. In Fig.5(d), the control line is finally depressurized, causing the membrane inside V1 to go back to its resting state. As a result, the air in M2 and M3 flows through V1 and out of the hole in M1, deflating the actuator (Fig.5(d)) and simulating what would occur had the valve not been present. The deflation of M2 and M3 took around 15 s due to the presence of V2 and V3 that, although not being active, still provide resistance to the flow, making the overall deflation transient longer.

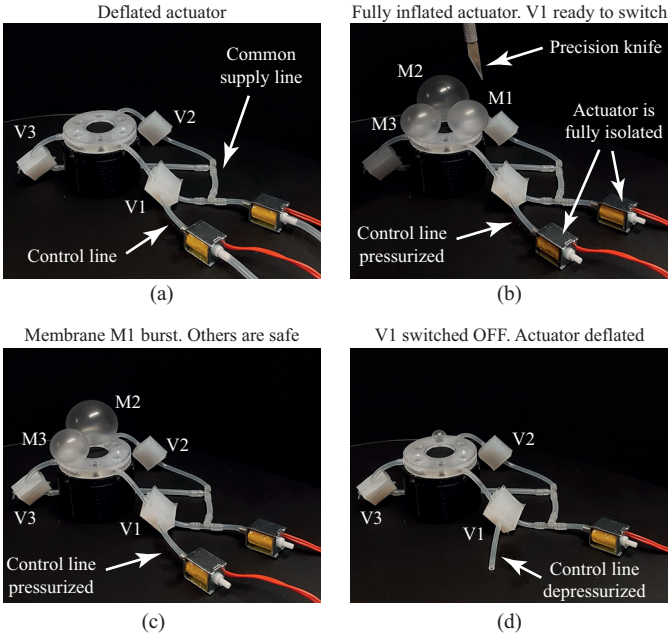

Fig. 5. Soft valves used with an inflatable actuator to demo fault isolation. (a) Soft pneumatic actuator ready for inflation. The three inlets are connected to the main supply through three soft valves. V1's control line is connected while V2 and V3 only ensure a similar level of resistance on all supply lines. (b) After inflation, the supply and control line valves are shut off and disconnected, isolating the actuator from the pump. The nonuniform inflation is due to manufacturing inaccuracies in the actuator. Membrane M1 is then burst using a precision knife. (c) The soft valve isolates the faulty membrane from the remaining ones, preventing their deflation. (d) The control line is discharged. In 15 s the actuator fully deflated, with air flowing from the intact membranes out through the cut in the faulty one, further proving the effect of the soft valve.

DISCUSSION AND CONCLUSION

In this paper, we presented a soft valve designed to readily isolate a burst section of a soft inflatable actuator before the fault can propagate to the rest of the system. No additional sensing is required, as the shut-off action of the valve is triggered by the fault itself. Combined with self healing techniques, it could either isolate a faulty segment while healing occurs or act as a fail safe alternative in case of unrecoverable damage. Untethered applications, where actuation fluid is limited, could also benefit from its use.

Some of the limitations that have emerged entail manufacturing and modelling. When using Ecoflex™ 00-50, achieving a thin uniform layer of Sil-poxy™ without affecting the small features of the valve proved to be challenging. Further investigation in bonding techniques may be needed to scale down the design. In comparison, PDMS proved to be a more accurate and time efficient alternative. Its higher stiffness, though, limits its application in inflatable soft robots. With respect to modelling, discrepancies between FEA and experimental results were observed and are likely to be linked to internal deformations upon pressurization and to the interaction between the air flow and the membrane. A thin membrane, 100 μm thick, granted the most reliable performance: the shut-off reaction was fast (less than 30 ms) and provided perfect sealing both during the preliminary tests as well as during the final application. In addition to the modelling aspects, future work will involve integrating the soft valve into the actuator, leading to a monolithic solution with less tubing and external rigid valves.

ACKNOWLEDGMENT

The authors acknowledge Quentin Lahondes for helping with the use of the oxygen plasma machine.

REFERENCES

[1] E. W. Hawkes, L. H. Blumenschein, J. D. Greer, and A. M. Okamura, "A soft robot that navigates its environment through growth," *Science Robotics*, vol. 2, no. 8, p. eaan3028, 2017.
[2] R. F. Shepherd *et al.*, "Multigait soft robot," *Proceedings of the National Academy of Sciences*, vol. 108, no. 51, pp. 20400–20403, 2011.
[3] M. T. Tolley *et al.*, "A resilient, untethered soft robot," *Soft Robotics*, vol. 1, no. 3, pp. 213–223, 2014.
[4] M. Baumgartner *et al.*, "Resilient yet entirely degradable gelatin-based biogels for soft robots and electronics," *Nature Materials*, vol. 19, pp. 1102–1109, Oct 2020.
[5] E. Perez-Guagnelli *et al.*, "Characterization, simulation and control of a soft helical pneumatic implantable robot for tissue regeneration," *IEEE Transactions on Medical Robotics and Bionics*, vol. 2, no. 1, pp. 94–103, 2020.
[6] B. Gorissen, D. Reynaerts, S. Konishi, K. Yoshida, J.-W. Kim, and M. De Volder, "Elastic inflatable actuators for soft robotic applications," *Advanced Materials*, vol. 29, no. 43, p. 1604977, 2017.
[7] H. Wang, M. Totaro, and L. Beccai, "Toward perceptive soft robots: Progress and challenges," *Advanced Science*, vol. 5, no. 9, p. 1800541, 2018.
[8] T. Kim, S. Lee, T. Hong, G. Shin, T. Kim, and Y.-L. Park, "Heterogeneous sensing in a multifunctional soft sensor for human-robot interfaces," *Science Robotics*, vol. 5, no. 49, p. eabc6878, 2020.
[9] M. Wehner *et al.*, "An integrated design and fabrication strategy for entirely soft, autonomous robots," *Nature*, vol. 536, pp. 451–455, Aug 2016.
[10] S. T. Mahon, A. Buchoux, M. E. Sayed, L. Teng, and A. A. Stokes, "Soft robots for extreme environments: Removing electronic control," *CoRR*, vol. abs/1903.10779, 2019.
[11] M. J. Ford *et al.*, "A multifunctional shape-morphing elastomer with liquid metal inclusions," *Proceedings of the National Academy of Sciences*, vol. 116, no. 43, pp. 21438–21444, 2019.
[12] S. Liu, O. Oderinde, I. Hussain, F. Yao, and G. Fu, "Dual ionic cross-linked double network hydrogel with self-healing, conductive, and force sensitive properties," *Polymer*, vol. 144, pp. 111–120, 2018.
[13] G. Cai, J. Wang, K. Qian, J. Chen, S. Li, and P. S. Lee, "Extremely stretchable strain sensors based on conductive self-healing dynamic cross-links hydrogels for human-motion detection," *Advanced Science*, vol. 4, no. 2, p. 1600190, 2017.
[14] S. Terryn, J. Brancart, D. Lefeber, G. V. Assche, and B. Vanderborght, "Self-healing soft pneumatic robots," *Science Robotics*, vol. 2, no. 9, p. eaan4268, 2017.
[15] R. F. Shepherd, A. A. Stokes, R. M. D. Nunes, and G. M. Whitesides, "Soft machines that are resistant to puncture and that self seal," *Advanced Materials*, vol. 25, no. 46, pp. 6709–6713, 2013.
[16] T. J. Wallin *et al.*, "Click chemistry stereolithography for soft robots that self-heal," *J. Mater. Chem. B*, vol. 5, pp. 6249–6255, 2017.
[17] P. Rothemund *et al.*, "A soft, bistable valve for autonomous control of soft actuators," *Science Robotics*, vol. 3, no. 16, p. eaar7986, 2018.
[18] D. Drotman, S. Jadhav, D. Sharp, C. Chan, and M. T. Tolley, "Electronics-free pneumatic circuits for controlling soft-legged robots," *Science Robotics*, vol. 6, no. 51, p. eaay2627, 2021.
[19] M. A. Unger, H.-P. Chou, T. Thorsen, A. Scherer, and S. R. Quake, "Monolithic microfabricated valves and pumps by multilayer soft lithography," *Science*, vol. 288, no. 5463, pp. 113–116, 2000.
[20] Y.-S. Lee, N. Bhattacharjee, and A. Folch, "3d-printed quake-style microvalves and micropumps," *Lab Chip*, vol. 18, no. 8, pp. 1207–1214, 2018.
[21] N. Herzig, J. Jones, E. Perez-Guagnelli, and D. D. Damian, "Model and validation of a highly extensible and tough actuator based on a ballooning membrane," in *2021 IEEE International Conference on Robotics and Automation (ICRA)*, pp. 11961–11967, 2021.